Discharge Characteristics of Small Sonic Nozzles in the Shape of Pyramidal Convergent and Conical Divergent

Chih-Chung HU[1], Win-Ti LIN[2], Chun-Min SU[3], Wen-Jay LIU[4]
[1,4]Department of Electronic Engineering, Kao Yuan University of Technology, Taiwan.
1821, Jhongshan Rd., Lujhu Township, Kaohsiung County 821, Taiwan 300, R.O.C.
[2,3]Center for Measurement Standards, Industrial Technology Research Institute, Taiwan
30, Ta Hsueh Road, Hsinchu, Taiwan 300, R.O.C.
Phone: 886-7-6077296, FAX: 886-7-6077000, E-mail: t10057@cc.kyu.edu.tw

Abstract: This study cooperated the KOH anisotropic etching with the laser machining to fabricate small sonic nozzles in the shape of a pyramidal convergent inlet followed by a conical diffuser with a divergent angle of 5^o. Three different diffuser lengths were made for the nozzles. The throat diameters were around 100 μm. Experiments were performed to obtain discharge coefficients and critical back pressure ratios in Reynolds numbers ranging from 5.8×10^2 to 4.5×10^3. The critical back pressure ratio for one of the nozzle type examined reached 0.486 at $Re = 4.4\times10^3$. Numerical simulations were also implemented to discover the flow fields at an upstream pressure of 203 kPa. The simulation results revealed that, besides flow separation, the first set of oblique shocks appeared in the nozzle jet could lead to tremendous pressure loss. The weaker of the oblique shocks, the higher the critical back pressure ratio would be obtained.

Keyword: Small Sonic Nozzle, Discharge Coefficient, Critical Back Pressure Ratio

1. Introduction

Small sonic nozzles, that is, throat diameter smaller than 200 μm, are found more and more in the measurement of gas flow. However, due to the small size, the geometries are quite difficult made to conform to the toroidal or cylindrical configuration in ISO 9300 [1], nor is the surface roughness. The fabrication techniques for small sonic nozzles may differ from conventional machining and the employed technique usually determines the achieved nozzle shape. The nozzles with shapes deviating from the ISO configurations and Reynolds numbers smaller than 2.1×10^4 must be calibrated before applying to flow measurement. Bignell [2] examined several non-ISO-typed sonic nozzles with throat diameters of 100 to 200 μm, including a shrinking glass tube, a water-cutting head, and a nozzle with rectangular throat. Nakao and Takamoto [3] studied quadrant sonic nozzles with throat diameters of 99 μm, 0.828 mm, and 1.203 mm. In contrast to conventional machining, MEMS technology is favored for micro devices. Mammana et al. [4] used an electro-chemical etching process to form a diamond nozzle with a throat diameter of 217 μm. Byat et al. employed the technique of deep RIE to fabricate micro thrusters for micro satellites [5, 6]. Their results [2-4] indicate that the non-ISO-typed sonic nozzles can be applied to standard flow systems.

Our previous studies [7, 8] employed the technique of KOH anisotropic etching to fabricate small sonic nozzles from a silicon wafer. Due to the nature of the anisotropic etching, the nozzles achieved had pyramidal convergent and divergent sections. The half angles were restricted to 35.3°, as shown in Fig. 1. The pyramidal nozzles were made in different sizes for the throat dimension, *d*, ranging from 38 to 188 μm. Four types of the nozzles were investigated for the discharge characteristics and size effect in Reynolds numbers ranging from 3×10^2 to 8×10^3. From the results [7, 8], the pyramidal silicon nozzles bear good properties in several aspects, like thermal response, maximum sustainable pressure, and long-term stability. However, the

pyramidal sonic nozzles have a divergent angle of 35.3°, much larger than the ISO-suggested 4° to 6°. On average, the *CBPR* (critical back pressure ratio) for the pyramidal sonic nozzles with convergent and divergent sections are between 0.33 and 0.36. The authors believe that the *CBPR* can be further improved as long as the nozzle divergent is redesigned.

Fabricating small sonic nozzles, *d* around 100 μm, with higher *CBPR*s is the main purpose of this study. A higher *CBPR* signifies that the nozzle is choked easily and operated at a higher back pressure ratio. Therefore, the fabrication methods employed here are a little different from our previous studies [7, 8]. The KOH anisotropic etching is utilized to fabricate the upstream convergent section of the nozzle. As for the downstream section, the technique of laser machining is applied to shaping a conical diffuser with a divergent angle of 5°. Figure 2 shows a schematic illustration of the configuration. The conical diffuser features the major difference in geometry from the pyramidal sonic nozzles in [7, 8]. The conical diffuser was made into three different lengths to study how it affects the pressure loss of the nozzle. Experiments were performed to find out the discharge coefficients and critical back pressure ratios. In parallel, numerical simulations by the commercial software, *Fluent* 6, were also implemented to calculate the flow fields.

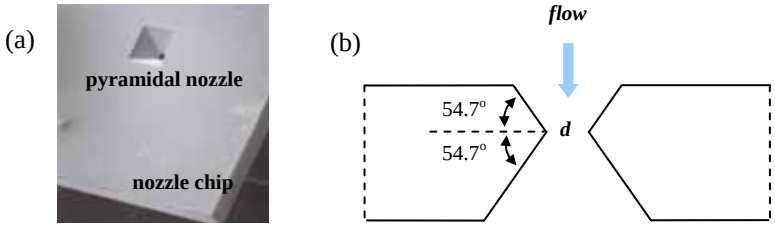

Fig. 1 The pyramidal sonic nozzle; (a) SEM picture, and (b) a sagittal view.

2. Fabrication of Silicon Sonic Nozzles

This study used the techniques of KOH anisotropic etching and laser machining to fabricate small sonic nozzle with the shape illustrated in Fig. 2. The KOH etching can result in good surface roughness, but the nozzle geometry is limited to pyramid [7-9]. The laser machining can shape the desired nozzle geometry, but the achieved roughness, so far, is poor. Concerning the surface roughness, the KOH anisotropic etching was utilized to form the upstream convergent section of a sonic nozzle. As mentioned above, the achieved convergent section would be like a pyramidal concave, resulting in a half angle of 35.3°. From [9], the etching condition of this study would lead to a surface roughness less than 40 nm. After the pyramidal concave being made, the laser machining was used to drill a cylindrical tube to penetrate the silicon wafer along the center line of the pyramidal concave. Then, the diffuser with a divergent angle of 5° was carved step by step. The surface roughness by the laser machining employed was about 5 μm, high enough to cause non-negligible disturbances to some micro channel flows. However, in this study, the flow separation or viscous boundary layer in the conical divergent might alleviate this roughness effect. Figure 3a shows the SEM (Scanning electron microscope) picture of the nozzle inlet or convergent section, and Fig. 3b is the exit of the conical diffuser. In the figure, the throat diameter, *d*, is about 113 μm.

The thickness of the silicon wafer employed was 525 μm. In other words, this is the length of the silicon nozzle. Figure 4 shows the sagittal views of the nozzles examined in this study. The nominal dimensions labeled in the figure are corresponding to the throat diameter of 100 μm. However, due to the fabrication uncertainty, the actual sizes obtained differ more or less from the nominal dimensions. The first one, called the A-L1 nozzle, bears a KOH-etched pyramidal inlet

and a laser-drilled cylindrical tube as outlet. The nominal length of the cylindrical tube is 39 μm, but it can not be measured. Its diameter, however, is estimated about 96 μm by SEM. As for the A-L2 nozzle, the pyramidal convergent section is followed by a cylindrical tube with a length of about 30 μm, and then a short conical diffuser with a length of about 37 μm and a divergent angle of 5°. The throat diameter, actually the diameter of the cylindrical tube, is about 82 μm, estimated by SEM. The third one, called the A-L3 nozzle, comprises a pyramidal convergent section, a cylinder tube (throat position), and a longer conical diffuser. The diffuser length of the A-L3 nozzle is 3.7*d*, about 9 times of the A-L2 nozzle's, which is expected to save more pressure recovery among the three nozzle types. The throat diameter of the A-L3 nozzle is measured about 113 μm, see also in Fig. 3. The last, called the B nozzle, has already been investigated in [7, 8]. Its convergent and divergent sections are both pyramidal. The side length of the nozzle throat is 94 μm. Its results are shown here to be compared with the other three nozzles made in this study.

Fig. 2 The nozzle with pyramidal convergent and conical divergent.

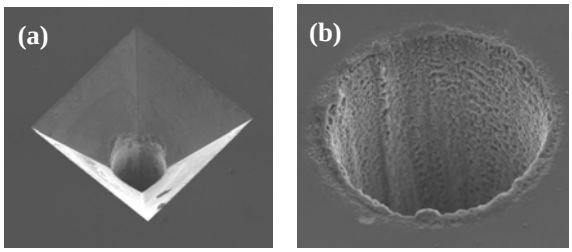

Fig. 3 Scanning electron microscope (SEM) pictures of the A-L3 nozzle; (a) the convergent section and (b) the exit of the nozzle diffuser. The throat diameter is 113 μm.

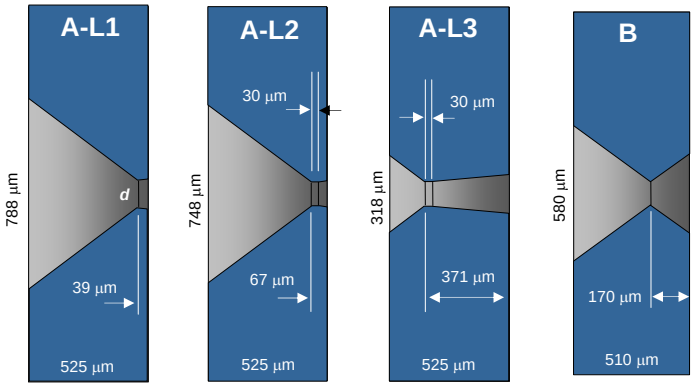

Fig. 4 Sagittal views of the nozzles examined.

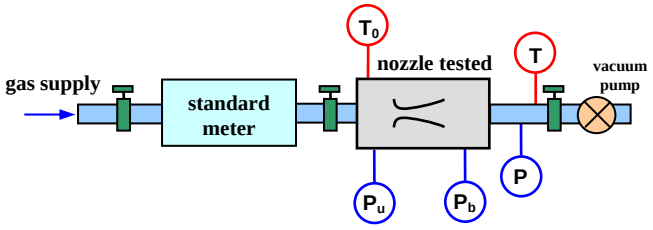

Fig. 5 Arrangement of the instrumentations in experiments.

3. Experimental Facilities

Experiments for the nozzles were performed in the Flow & Energy Research Laboratory of the Center for Measurement Standards, Industrial Technology Research Institute (CMS/ITRI), Taiwan. The employed instrumentations are the same as those in our previous study [7, 8]. Therefore, a detail description is not given here. Since the small sonic nozzles were made of

silicon crystal, a special clamping holder must prevent the nozzle chip from fractures. The clamped nozzle chip was installed in a straight circular conduit with a diameter D =14 mm. A laminar flow element was installed in the upstream of the nozzle set to measure the mass flow rate, as shown in Fig. 5. The pipeline in the downstream side was connected to a vacuum pump for a controllable back pressure. The relative standard uncertainty is 0.11 % for the measurement of mass flow rate in the range of 0.04 to 480 mg/s. The throat dimensions of the sonic nozzles were obtained from a scanning electron microscope (SEM). The uncertainty of the throat dimension is estimated about 2 % in maximum, leading to an uncertainty of about 4 % of the discharge coefficients.

4. Experimental Results

Calibrating discharge coefficient, *Cd*, of a sonic nozzle is very important before applying the nozzle to flow measurement. The *Cd* represents the ratio of real mass flow rate to ideal mass flow rate in sonic condition. Figure 6 gives the data of *Cd* versus *Re* for the four nozzles shown in Fig. 4. The *Re* represents the real Reynolds number, based on the mass flow rate actually measured and the throat dimension, *d*. In experiments, the upstream pressure was controlled to the values between 100 and 300 kPa to obtain different *Re* and the *Cd*. The downstream pressure, for convenience, is kept at 0.6 kPa to ensure the choke conditions for each upstream pressure.

In Fig. 6, the A-L3 nozzle has a higher *Cd* curve, shown by the triangular symbol, than the others. The A-L2 is the lowest, shown by the circular symbol. However, the data are insufficient to describe how the nozzle configuration affects the *Cd* curve. Our previous study [8] shows that both the nozzle configuration and throat size influence the *Cd* result. As seen in the figure legend, the A-L3 nozzle has the largest throat size actually. Therefore, it is not determined whether the higher *Cd* curve of the A-L3 nozzle results from its configuration or its larger throat size. Numerical simulations shown later might provide a reasonable comparison of the *Cd*s for the nozzles with the same throat dimension. For the A-L1 nozzle, shown by the square symbol, the *Cd* data have a very good linearity to $Re^{-0.5}$ with an error less than ±0.03%. As for the other three, their *Cd* data all have a good linearity to $Re^{-0.7}$ with an acceptable error less than ±0.1%.

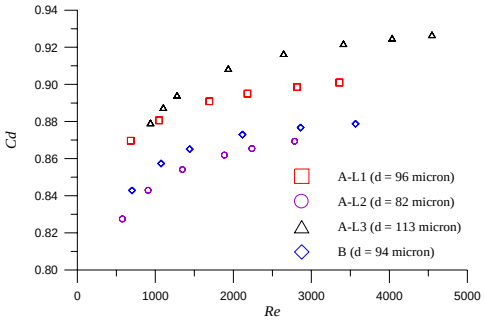

Fig. 6 Cd versus Re.

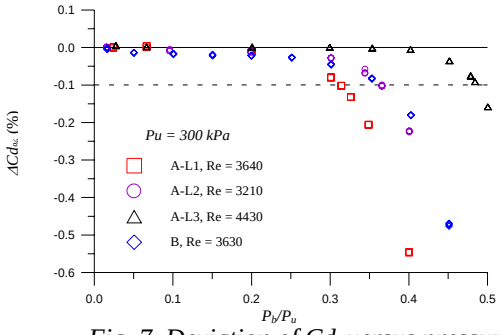

Fig. 7 Deviation of Cd_i versus pressure ratio at P_u = 300 kPa.

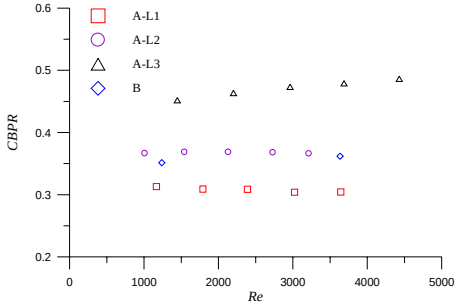

Fig. 8 CBPR versus Re.

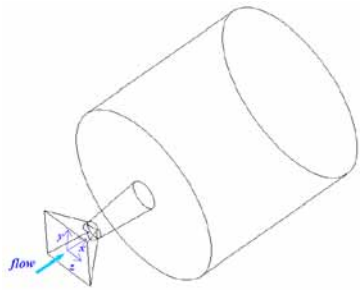

Fig. 9 Computation domain of the A-L3 nozzle and the coordinate system.

Maintaining the choked condition is crucial while measuring the flow rate by a sonic nozzle. The ratio of downstream pressure to upstream pressure is often utilized to monitor if the nozzle is properly choked. When the pressure ratio is higher than a critical value, usually called the critical back pressure ratio (*CBPR*), the sonic nozzle will lose its choked condition. For the *CBPR* in this study, a given upstream pressure, P_u, was set, and the downstream pressure, P_b, would start at a very low value, i.e. P_b/P_u smaller than 0.025, to obtain a reference *Cd*, saying Cd_0. P_u and P_b were measured in the flow conduit at 1*D* (*D* = 14 mm) upstream and 1*D* downstream of the nozzle [8]. After that, the downstream pressure was increased gradually to obtain the other Cd_i at different pressure conditions. As known, the Cd_i deviates gradually from the Cd_0 as the downstream pressure increasing. $\Delta Cd_{\%}$ is defined as follows to describe this deviation.

$$\Delta Cd_{\%} = \frac{Cd_i - Cd_0}{Cd_0} \times 100\% \quad (1)$$

Figure 7 gives the results of $\Delta Cd_{\%}$ for P_u around 300 kPa. The symbols employed are the same as those in Fig. 6. For the A-L3 nozzle, the deviation can be neglected as P_b/P_u smaller than 0.4. After that, the $\Delta Cd_{\%}$ decays gradually. As it reaches -0.1%, the pressure ratio is defined as the *CBPR* [3, 7, 8], signifying the unchoked condition. With this definition, the *CBPR* for the A-L3 nozzle is 0.486 at P_u = 300 kPa or $Re = 4.4\times10^3$. They are 0.304, 0.366, and 0.362 for the A-L1, A-L2, and B nozzles, respectively. The results are consistent to our expectation. The A-L3 nozzle with the longest diffuser and a divergent angle of 5^o leads to the largest *CBPR*, implying the least pressure loss. The A-L1 nozzle without any diffuser performs the poorest.

Likewise, the *CBPR*s for the nozzles at the other Reynolds numbers are found and shown in Fig. 8. For the A-L1 and A-L2 nozzles, the *CBPR*s are insensitive to *Re*. The average values are 0.308 and 0.367, respectively. For the A-L3 nozzle, the *CBPR* increases from 0.452 to 0.486 with *Re*. Averagely speaking, the *CBPR* of the A-L3 nozzle is improved by 35.3% compared with the B nozzle [7, 8]. On the other hand, the *CBPR*s for the A-L2 and B nozzles are comparable. The A-L1 nozzle, as mentioned above, has the poorest. In [3], the *CBPR* for the quadrant nozzle with d = 99 μm is varied from 0.1 to 0.26 for $Re = 10^2$ to 10^3, and with d = 0.828 mm it is 0.2 to 0.42 for $Re = 10^2$ to 8×10^3.

5. Numerical Results

Numerical simulations of the four nozzle configurations were implemented to investigate the flow fields by the software *Fluent* 6. Compressible and steady-state conditions were assumed for solving the Reynolds-averaged Navier-Stokes equations. Though most of the field would be laminar, the downstream jet evolves into turbulence easily. Our previous study [8] evaluated the turbulence models of Spalart-Allmaras and standard k-ω [10-12] to predict the discharge characteristics of the B nozzle. The results indicated that the Spalart-Allmaras turbulence model could provide closer values to the experimental data. Therefore, this study employed the Spalart-Allmaras turbulence model.

The dimensions of the nozzles followed those shown in Fig. 4. Notably, the throat dimension, *d*, for the four nozzles were all set at 100 μm. The upstream and downstream flow conduits (*D* = 14 mm) for the nozzle were excluded. In the experiments, a cylindrical tube with a diameter of 2 mm and a length of 3 mm was present between the nozzle and the downstream conduit. In the simulations, the diameter and the length of the tube were both reduced to 1 mm to lower the total grid number for saving computation time. However, it would sacrifice some simulation accuracy near the exit of the computation domain. Figure 9 shows the computation domain for the A-L3

nozzle. The system origin is placed at the center of the inlet plane. x represents the streamwise direction, and y and z representing the vertical and lateral axes, respectively. Boundary-layer meshing technique was adopted to enhance the spatial resolution in the viscous boundary layer. The model constructions and coordinate systems for the other three nozzles followed the same criterions as those of the A-L3 nozzle. The inlet total pressure, P_t, was set at 2 atm (2.03 bar or 203 kPa) and the outlet pressure, P_b, was 0.4 atm. The temperature was set at 296 K at the inlet and outlet planes. The Knudsen numbers for these cases were smaller than 0.01, implying that the flow was continuous and no-slip condition was applicable [13].

The computation errors must be estimated before showing the obtained flow patterns. The experimental data of Cd at P_u = 203 kPa may be used to compare with the simulation results. The P_u measured in experiments can be approximately regarded as the P_t. However, the throat sizes in experiments are not exactly the same as those in simulations, which must be considered while evaluating the computing accuracy by the readers. As an illustration, the Cd computed for the A-L1 nozzle is 0.906 with Re = 2435, and the Cd obtained at experiment is 0.8966 (d = 96 μm). A direct comparison suggests the computation will have an error less than 1% if the throat dimensions are the same in the experiment and simulation. The Cds computed for the A-L2 and A-L3 nozzles are 0.903 and 0.90, respectively. As found, the A-L1 configuration results in the highest Cd value among them. The result seems to indicate that the longer of the diffuser results in a higher Cd. However, it is cautionary that the difference of Cd among them is so small and within the computation uncertainty.

Figure 10 gives the contours of streamwise velocity, V_x, on the x-y plane at z = 0 for the four nozzles. These pictures clearly show the flow patterns. See Fig. 10a for the A-L1 nozzle. The jet flow in the core region experiences acceleration and deceleration in turn as it travels downstream. It behaves like an under-expanded supersonic nozzle flow [8, 13]. The expansion fans appeared right downstream of the throat exit accelerate the sonic flow to about M = 2.78 at x/d = 6.41. Then, oblique shocks slow down the flow. At least four sets of expansion and oblique shock waves can be clearly recognized in this figure. Similar flow patterns can be found in the other three cases.

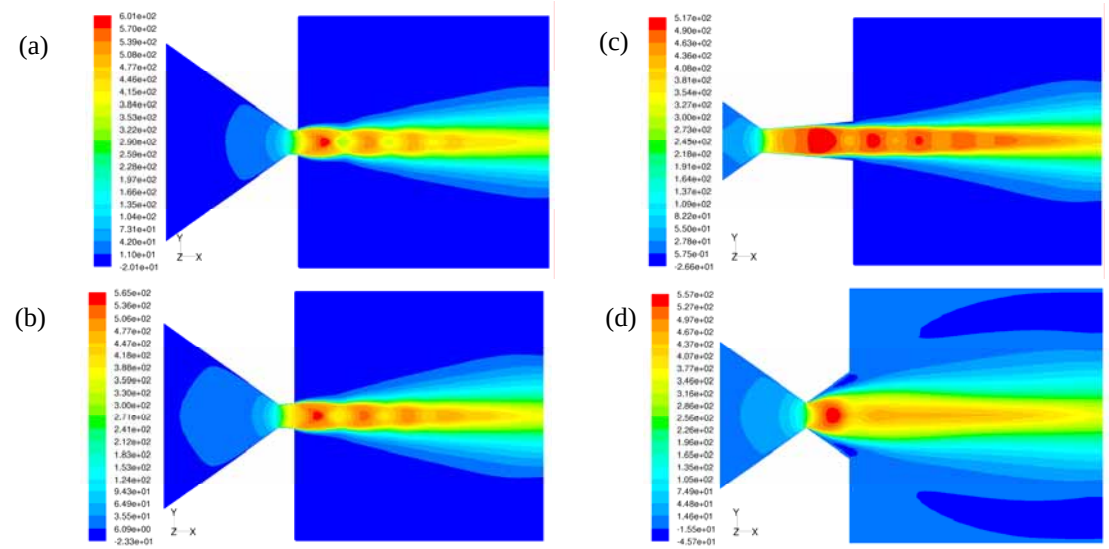

Fig. 10 Contours of V_x on the x-y plane at z = 0 at P_u = 203 kPa for the nozzles of (a) A-L1, (b) A-L2, (c) A-L3, and (d) B.

The jet flows for the A-L1 to A-L3 nozzles are more confined in the core region and persist a longer distance in the downstream, compared with that of the B nozzle. Unlike the A-L1 to A-L3,

the type B nozzle doesn't have a straight tube at the throat position to restrict the flow to the streamwise direction. Instead, the sharp-edged throat and the large divergent angle (35.3°) result in a low-speed separation region between the high speed core and the diffuser wall [8]. The recirculation zone in the downstream tube is also seen broader than those of the A-L1 to A-L3.

Figure 11a gives the Mach number variations along the centerlines of those planes in Fig. 10. Figure 11b shows the corresponding total pressure, P_t. The expansion fans and oblique shocks, appeared in Fig. 10, cause the Mach number in Fig. 11a to increase and decrease alternatively. For the A-L1 nozzle shown by the square symbol, the flow reaches the sonic condition at x/d = 5.21, quite near the throat exit. The flow then suffers an abrupt expansion to reach a highest Mach number among the four nozzles. For the A-L2 nozzle shown by the circular symbol, the sonic condition occurs at x/d = 4.93, about 0.05d behind the throat exit. The flow of the A-L2 nozzle also keeps accelerating after the throat. However, the short diffuser alleviates the expansion of the flow. The Mach number variation is smaller than that of the A-L1 nozzle, signifying a weaker structure of expansion fans and oblique shocks.

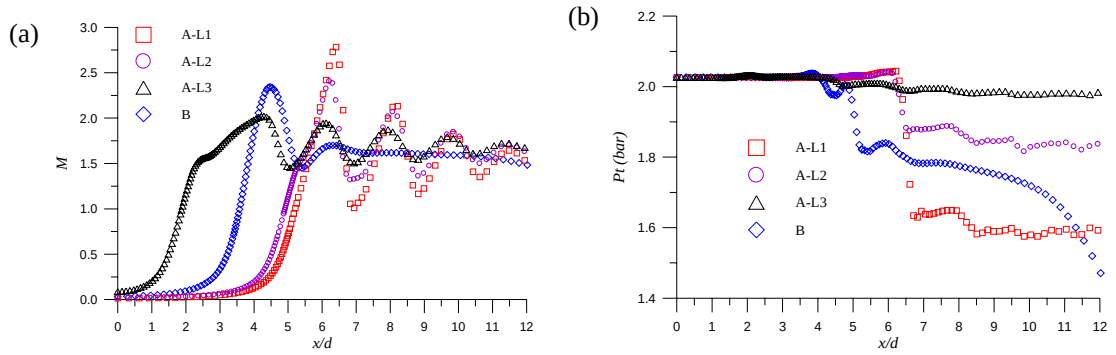

Fig. 11 (a) Mach number and (b) total pressure variations along the centerline.

As for the A-L3 nozzle, the longer diffuser leads to the mildest flow acceleration and deceleration among the nozzles. Referring to Fig. 11b, this mildest variation of Mach number brings the least loss of total pressure. A common situation for the A-L1 to A-L3 nozzles is that the first set of oblique shocks appeared causes the major loss of total pressure. For the A-L1 case, the loss by the first shocks is about 20% of the inlet total pressure. For the A-L2 and A-L3 nozzles, the losses are 8.4% and 0.98%, respectively. The B nozzle also has a large loss by the first shocks, about 10.3%. Unlike the results of the A-L1 to A-L3 nozzles, the variations of Mach number and total pressure for the B nozzle reveal that the structure of expansion fans and oblique shocks dissipates sooner than the others. The total pressure at the core region starts to decay in a more upstream position. This is explained that the stronger recirculation in the downstream tube of the B nozzle enhance the momentum diffusion between the core region and the surrounding flow.

The simulation results help to explain the experimental data in Figs. 7 and 8. It tells that, besides flow separation, shocks appeared in the downstream jet can also bring tremendous pressure loss. A proper diffuser that avoids flow separation and generates weak shocks will save more pressure recovery and improve the *CBPR* of a small sonic nozzle. However, fabricating such a diffuser in micro scale is never an easy task.

6. Conclusion

Small sonic nozzles with throat dimensions around 100 μm were made by the KOH anisotropic etching and the laser machining. The nozzles achieved had the shape of a pyramidal convergent inlet followed by a conical diffuser with a divergent angle of 5°. The conical divergent was the major difference from our previous pyramidal sonic nozzles [7, 8]. Three nozzles with different

diffuser lengths were investigated. The A-L1 nozzle bears a KOH-etched pyramidal inlet and a laser-drilled cylindrical tube as outlet. The A-L2 nozzle is similar to A-L1 nozzle, but a short conical diffuser with a length of about 0.37*d* and a divergent angle of 5° was added to the throat exit. The conical diffuser for the A-L3 nozzle had a length of 3.7*d*. The *Cd* curves and the *CBPR*s were examined experimentally for *Re* ranging from 5.8×10^2 to 4.5×10^3. The results showed that the *CBPR*s for the A-L1 and A-L2 nozzles were insensitive to *Re*. Their average values were 0.308 and 0.367, respectively. For the A-L3 nozzle, the *CBPR* increased from 0.452 to 0.486 with *Re*, which was improved averagely by 35.3% compared with the B nozzle in our previous study [7, 8]. It tells that, even for a small sonic nozzle with a diameter of 100μm or below, a diffuser with a proper divergent angle and length is still necessary for improving the *CBPR*.

Numerical simulations of the nozzles were implemented at an upstream total pressure of 203 kPa. The computation error estimated from the experimental data was less than 1%. Though the computation domain was quite simplified from the real pipelines, the flow fields obtained revealed some interesting phenomena. The first was that the *Cd*s computed for the A-L1 to A-L3 nozzles were influenced by the diffuser length. It was speculated that the longer the diffuser length the smaller the *Cd* value. The second was that the first set of the oblique shocks leaded to tremendous pressure loss. The total pressure losses caused by the first shocks were about 20%, 8.4% and 0.98% for the A-L1, A-L2, and A-L3 nozzles, respectively. The results explained the experimental data. Once again, it reinforces the importance of a proper diffuser. A proper diffuser for a small sonic nozzle must avoid flow separation and yield shocks as weak as possible to save more pressure recovery. Therefore, fabricating such a diffuser in micro scale becomes the crucial problem to be solved.

Acknowledgements

The authors acknowledge the funding support of National Science Council, Taiwan, on this work, under the contract number NSC99-2221-E-244-006-.

Reference

[1] ISO 9300: Measurement of gas flow by means of critical flow Venturi nozzles, 2003.
[2] Bignell, N., Using small nozzles as secondary flow standards. Flow Measurement and Instrumentation 11, 329-337, 2000.
[3] Nakao, S., Takamoto, M., Choking phenomena of sonic nozzles at low Reynolds numbers. Flow Measurement and Instrumentation 11, 285-291, 2000.
[4] Mammana, S. S., Salvadon, M. C., Characterization of diamond sonic micronozzles and microtube. J. Vac. Sci. Technol. B 21(5), 2034-2037, 2003.
[5] Bayt, R. L., Ayon, A. A., Breuer, K. S., Performance evaluation of MEMS-based micronozzles. 33rd AIAA/ASME/SAE/ASEE Joint Propulsion Conference & Exhibit, AIAA paper 97-3169, July 7-9, 1997.
[6] Bayt, R. L., Breuer, K. S., Systems design and performance of hot and cold supersonic microjets. 39th AIAA Aerospace Science Meeting and Exhibit, AIAA paper 2001-0721, January 8-11, 2001.
[7] Hu, C. C., Lin, W. T., Performance test of KOH-etched silicon sonic nozzles, Flow Measurement and Instrumentation, 20, pp. 122-126, 2009.
[8] Hu, C. C., Lin, W. T., ans Su, C. M., Flow Characteristics of Pyramidal Shaped Small Sonic Nozzles, submitted to Flow Measurement and Instrumentation (in revision).
[9] Madou, M. J., Fundamentals of microfabrication, CRC Press, Boca Raton, New York, 1997.
[10] Wilcox D. C., Turbulence Modeling for CFD, 2nd edition, DCW Industries, Inc., 1998.
[11] Wilcox D. C., Turbulence Modeling: An overview, AIAA Paper 2001-0724, 2001.
[12] Fluent User's Guide, Fluent Inc., 2005.
[13] James, E. A., Gas dynamics, second edition, Ally and Bacon, 1984.